(This is a sample cover image for this issue. The actual cover is not yet available at this time.)

Remote Sensing of Environment 124 (2012) 742–755

Contents lists available at SciVerse ScienceDirect

Remote Sensing of Environment

journal homepage: www.elsevier.com/locate/rse

Characterizing spatial representativeness of flux tower eddy-covariance measurements across the Canadian Carbon Program Network using remote sensing and footprint analysis

Baozhang Chen [a,b,*], Nicholas C. Coops [b], Dongjie Fu [a], Hank A. Margolis [c], Brian D. Amiro [d], T. Andrew Black [e], M. Altaf Arain [f], Alan G. Barr [g], Charles P.-A. Bourque [h], Lawrence B. Flanagan [i], Peter M. Lafleur [j], J. Harry McCaughey [k], Steven C. Wofsy [l]

[a] LREIS Institute of Geographic Sciences & Nature Resources Research, Chinese Academy of Sciences, Beijing 100101, China
[b] Department of Forest Resource Management, 2424 Main Mall, University of British Columbia, Vancouver, Canada V6T 1Z4
[c] Faculté de Foresterie, de Géographie et de Géomatique, Université Laval, Québec, Canada G1K 7P4
[d] Department of Soil Science, University of Manitoba, Winnipeg, Manitoba, Canada R3T 2N2
[e] Faculty of Land and Food Systems, 2357 Main Mall, University of British Columbia, Vancouver, Canada V6T 1Z4
[f] School of Geography and Earth Sciences and McMaster Center For Climate Change, McMaster University, Hamilton, Ontario, Canada L8S 4K1
[g] Climate Research Branch, Meteorological Service of Canada, Saskatoon, Saskatchewan, Canada S7N 3H5
[h] Faculty of Forestry and Environmental Management, University of New Brunswick, Fredericton, New Brunswick, Canada E3B 6C2
[i] Department of Biological Sciences, University of Lethbridge, Lethbridge, Alberta, Canada T1K 3M4
[j] Department of Geography, Trent University, Peterborough, Ontario, Canada K9J 7B8
[k] Department of Geography, Queen's University, Kingston, Ontario, Canada K7L 3N6
[l] Department of Earth and Planetary Science, Harvard University, Cambridge, MA 02138, USA

ARTICLE INFO

Article history:
Received 27 May 2011
Received in revised form 29 May 2012
Accepted 3 June 2012
Available online xxxx

Keywords:
Fluxnet
Footprint climatology
Spatial representativeness
Eddy-covariance
Remote sensing

ABSTRACT

We describe a pragmatic approach for evaluating the spatial representativeness of flux tower measurements based on footprint climatology modeling analyses of land cover and remotely sensed vegetation indices. The approach was applied to the twelve flux sites of the Canadian Carbon Program (CCP) that include grassland, wetland, and temperate and boreal forests across an east–west continental gradient. The spatial variation within the footprint area was evaluated by examining the spatial structure of Normalized Difference Vegetation Index (NDVI) and land cover using geostatistical analyses of frequency distribution, variogram and window size. The results show that at most sites (i) the percentages of the target vegetation functional type (dominant land cover) observed by the CCP towers were higher than 60%; (ii) to some extent, most of the CCP sites presented anisotropically distributed patterns of NDVI in the 90% annual footprint climatology area; and (iii) the land surface heterogeneity within the flux footprint area differed among sites. Overall, the forest sites had larger fine-scale spatial variation than the grassland and wetland sites. The coniferous boreal forest sites had greater spatial variability than the two wetland sites and a coniferous temperate forest site. We conclude that the combination of footprint modeling, semivariogram and window size techniques, together with moderate spatial resolution remotely-sensed image data, is a pragmatic approach for assessing the spatial representativeness of flux tower measurements.

1. Introduction

The eddy covariance (EC) technique is commonly used to measure CO_2, water vapor and energy exchange between the atmosphere and terrestrial ecosystems (Baldocchi, 2008). The use of the EC technique to estimate surface exchange is based on the assumption that the contributing area of the fluxes (i.e. footprint area) is topographically flat and the vegetation extends uniformly (Baldocchi, 2003, 2008; Finnigan et al., 2003; Foken & Wichura, 1996). In reality however, there are few such ideal sites, with spatial heterogeneity generally causing problems in data quality, data analysis, and proper interpretation of EC-data (Sogachev et al. 2004). These problems can be addressed if the spatial representativeness of the measurements is known.

Individual towers provide information on the gas exchange between vegetation and the atmosphere which is assumed to be characteristic for a given ecosystem of interest (a target ecosystem) (Schmid & Lloyd, 1999). On this basis, networks of EC systems have been set up at biome, national, continental, and global scales based loosely

* Corresponding author at: Department of Forest Resource Management, University of British Columbia, 2424 Main Mall, Vancouver, Canada V6T 1Z4. Tel.: +1 604 822 6592; fax: +1 604 822 9106.
E-mail addresses: bobchen@interchange.ubc.ca, baozhang.chen0808@gmail.com (B. Chen).

0034-4257/$ – see front matter © 2012 Elsevier Inc. All rights reserved.
doi:10.1016/j.rse.2012.06.007

on the idea that individual nodes are representative of larger ecosystems (Baldocchi, 2008). However, utilization and application of EC measurements (especially for spatial up-scaling to landscape and regional scales) can be problematic due to difficulties/uncertainties in understanding/interpreting the long-term EC measurements (Chen et al., 2009a; Gockede et al., 2004; Rebmann et al., 2005). The spatial variation within the EC flux footprint area needs to be assessed prior to the data from these networks being combined with remote sensing data and/or ecosystem models to determine spatial and temporal variability of CO_2 exchanges over heterogeneous landscapes that have undergone some prior disturbance (e.g., land management, extreme weather, insect infestation, fire, etc.), or that contain different stand ages, species types (e.g., Heinsch et al., 2006).

Footprint models have been developed to estimate the probability of fluxes originated from a particular place surrounding the tower. The spatial variability of the source strength is usually controlled by the surface vegetation characteristics and soil conditions. It is assumed that the spatial variability of vegetation density is significantly correlated with that of the source flux strength (Kim et al., 2006). The combination of footprint modeling and remotely-sensed high-resolution image data is then proposed to characterize the heterogeneity over the EC flux footprint area (Chen et al., 2009a; Kim et al., 2006).

In this paper, we present a method to combine remotely sensed vegetation indices, a widely used land cover map, and a footprint model to characterize the source of the EC fluxes. This methodology was applied to the 12 main study sites of the Canadian Carbon Program (CCP) network (previous Fluxnet Canada Research Network). The footprint climatology, i.e. footprint estimates for long-term EC measurements, was calculated using the Simple Analytical Footprint model on Eulerian coordinates (SAFE-F, Chen et al., 2009a). A vegetation index (NDVI: Normalized Difference Vegetation Index) is generally related to green vegetation cover or vegetation canopy density. NDVI is also considered to be a relative and indirect indicator of photosynthetic capacity and is sometimes corrected with biophysical parameters such as green leaf biomass (e.g., Govind et al., 2009; Myneni et al., 1995; Sellers, 1985) and the fraction of green vegetation cover (Myneni et al., 1995). The NDVI used as a surrogate of the land-surface flux was derived from Landsat Thematic Mapper (TM) or Enhanced TM (ETM+) imagery data. The spatial variation within the footprint climatology area was evaluated by examining the spatial structure of the vegetation index and land cover using geostatistical measures, including the frequency distribution, variogram and window-size analyses.

2. Methods and data

2.1. Site characteristics

We selected 12 main flux tower sites of the CCP distributed along an east–west continental transect in Canada (Fig. 1). These sites cover four major biome types (grassland, wetland and both temperate and boreal forests) and six ecoregions (from west to east: Pacific maritime, prairies, boreal plains, boreal shield, mixed wood plains and Atlantic maritime). Site and EC flux tower characteristics are summarized in Table 1 (http://www.fluxnet-canada.ca).

2.2. Footprint and footprint climatology modeling

The footprint probability distribution function (PDF) of the measured fluxes can be estimated with footprint models (e.g., Schmid, 1994; Kljun et al., 2004; Chen et al., 2009a). However, the complexity and large computational demand of some models restricts their practical applicability. For multi-site EC datasets, it is advantageous to use a somewhat simplified footprint model that still retains the ability to discern spatial footprints. In this study we used the Simple Analytical Footprint model on Eulerian coordinates for scalar Flux (SAFE-F, Chen et al., 2009a) to compute the footprint PDF. This analytical footprint model takes into account atmospheric stability and uses the wind velocity power law above the canopy, allowing it to be applicable to a wide range of atmospheric conditions.

The SAFE-F model input includes the EC sensor height (h_m), canopy height (h_c), roughness length (z_0), friction velocity (u), u threshold for EC flux calculation (u_*^{th}), wind direction (WD), wind speed (u), standard deviation of lateral wind speed (σ_v), and sensible and latent heat fluxes measured at the EC sensor height. The input meteorological variables were measured in 2006, which was generally considered a normal weather year over most of the sites. These data were acquired from the CCP database (http://www.fluxnet-canada.ca/). Missing flux and meteorological data were filled using the gap-filling method of Chen et al. (2009b). The input land surface parameters h_m and h_c were taken from the literature as shown in Table 1 and z_0 is approximated as 10% of h_c (Raupach, 1994).

The EC flux community has recognized that the EC technique often underestimates nighttime net ecosystem exchange (NEE) during periods when turbulent mixing is insufficient (e.g. Black et al., 2000; Goulden et al., 1996; Jarvis et al., 1997). For a practical solution, these data obtained during calm, nocturnal periods are filtered using friction velocity as an indicator by many research groups. Similarly, the periods with low turbulence should be excluded in footprint calculation. The determination of an adequate u_*^{th} is crucial, however at present; there is no commonly accepted method to determine the adequate u_*^{th}. In the literature, researchers often find the u_*^{th} by visually examining the scatter plot of nighttime fluxes versus u_*: the threshold is located where the flux begins to level off as u_* increases. Because the EC fluxes measured during nighttime often appear to be rather noisy in the NEE versus u_* scatter plot, it is common that no clear patterns can be recognized visually (Gu et al., 2005). Even when there are easily identifiable patterns, the selection of u_*^{th} depends on the operator's subjectivity. To overcome such problems, different alternative heuristic methods have been proposed to automatically determine the appropriate u_*^{th} (Gu et al., 2005; Reichstein et al., 2003, 2005), but the uncertainty of the determination of u_*^{th} is still considerable. There is no basis to think that u_*^{th} is constant over time. It may well depend on leaf area distribution, stem density, canopy height, as well as meteorological conditions and terrain characteristics. Consequently, employing a single u_*^{th} all the time may also introduce biases (Papale et al., 2006). For all the 12 CCP flux tower sites, however, the u_*^{th} value is determined by each tower operator and treated as a constant over time.

There is a need to minimize methodological uncertainties introduced by the different u_* threshold selection procedures for the purpose of site intercomparisons. To determine the time-varying u_*^{th} for footprint calculation using the SEAF-F model, we applied a standardized method proposed by Papale et al. (2006) to all the 12 CCP sites. Briefly, the annual raw dataset was first divided into four seasons (January–March, April–June, July–September and October–December) and the each season's dataset was further split into six temperature classes with equal sample size: the threshold for each temperature class was only accepted if u_* is not or only weakly correlated with temperature ($|r|<0.4$), and the final threshold for each season was defined as the median of the thresholds of the (up to) six temperature classes. The standardized time-varying u_*^{th} values which were used in the SEAF-F model for individual CCP sites are different from those time-constant values determined by the tower operators (Table 1).

The model was run at half-hourly time steps at a grid size of 30×30 m (consistent with the Landsat spatial resolution) covering the domain area (6×6 km) centered on the towers. The half-hourly footprint PDFs were rotated along the wind direction and then accumulated to yield monthly, seasonal or annual values, of the footprint climatology.

The cumulative percentage footprint was calculated by: (i) sorting the footprint climatology in a descending order; and (ii) accumulating its value from the largest to the smallest. The detailed description

Fig. 1. Locations of flux sites of the Canadian Carbon Program (CCP) and eco-region distributions of Canada's landmass. For description of flux sites, see Table 1.

of the footprint model and the footprint climatology calculations are given in Chen et al. (2009a, 2011).

2.3. Land cover classification and analysis

Land cover for Canada's forested landmass was derived from Landsat data, jointly by the Canadian Forest Service and the Canadian Space Agency (Wulder et al., 2003). The methodology involved the unsupervised classification, hyperclustering, and manual labeling of Landsat data, facilitating the classification of land cover types (Franklin and Wulder, 2002; Slaymaker et al., 1996; Wulder et al., 2003).

In the Earth Observation for Sustainable Development of forest (EOSD) product, 23 unique land cover classes (Table 2) were represented and mapped at a spatial resolution of 25 m representing circa year 2000 conditions (Wulder et al., 2008). The accuracy of the EOSD product was reported to be 77%, approaching a target accuracy of 80%, with a 90% confidence interval of 74–80% (see Wulder et al., 2007). EOSD land cover products were acquired at each of the ten available sites with a 6×6 km area centered at individual tower location downloaded from the EOSD data portal (http://www4.saforah.org/eosdlcp/nts_prov.html) and were then resampled to 30 m resolution using a nearest neighbor approach. The Landsat land cover data for two of the twelve sites (ON-WPP39 and AB-GRS) are not available from EOSD since they are considered to be outside of the forested area of Canada.

For characterization of the CCP EC tower sites, the 23 land cover classes of EOSD products were aggregated into 8 broad vegetation functional types (Table 2).

We used histogram and frequency distribution analyses to represent the heterogeneity of land cover within the flux footprint area.

2.4. Analysis of Landsat images

Landsat imagery data acquired in 2006, or as close as possible, were acquired at each of the twelve sites with a 6×6 km area centered at individual tower locations downloaded from the U.S. Geological Survey (http://glovis.usgs.gov/). The scene path and row and the acquisition dates are shown in Table 3.

The Landsat imagery was georeferenced and atmospherically corrected using the cosine approximation model (COST) of Wu et al. (2005) and radiometrically normalized following Hall et al. (1991) for the inter-site comparison. The spectral index (NDVI) was then calculated following Tucker (1979) and Field et al. (1995) to describe the land surface heterogeneity.

2.5. Semivariogram

The semivariogram is commonly used in geostatistical remote-sensing applications (e.g., Atkinson, 1997; Atkinson and Lewis, 2000; Berberoglu et al., 2000, 2007; Curran, 1988; Curran and

Table 1
List of abbreviations, site characteristics and tower measurement information for the CCP sites [a].

Vegetation function type[b]	Site ID[c]	Eco-region	Latitude (°N)	Longitude (°W)	*LAI* ($m^2 m^{-2}$)	T_e (year)	h_m (m)	h_c (m)	u ($m s^{-1}$)	$u_*^{th}(EC)$ ($m s^{-1}$)	$u_*^{th}(FP)$ $\mu\pm\sigma$ ($m s^{-1}$)	H_e (m)	References
CBF	MB-NOBS	Boreal shield	55.87956	98.48084	4.1	1845	29	9.1	3.3	0.25	0.25±0.06	259	Dunn et al. (2007) and Turner et al. (2003)
	QC-EOBS	Boreal shield	49.69247	74.34204	3.7	1898	24	13.8	2.6	0.25	0.23±0.07	387	Richardson et al. (2006)
	SK-OJP	Boreal plains	53.91634	104.69203	3.4	1929	29	13.7	3.0	0.35	0.36±0.09	579	Barr et al. (2006)
	SK-SOBS	Boreal plains	53.98717	105.11779	5.6	1879	25	13.7	3.3	0.35	0.33±0.10	629	Barr et al. (2006)
CMF	NB-OBF	Atlantic maritime	46.47388	67.09937	8.4	1967	18.5	14	2.9	0.40	0.42±0.08	341	Xing et al. (2007)
CTF	BC-DF49	Pacific maritime	49.86883	125.33508	6.1	1949	43	33	1.8	0.30	0.28±0.07	320	Chen et al. (2009b)
	ON-WPP39	Mixed wood plains	42.71222	80.3572	8.0	1939	28	21.8	2.4	0.35	0.33±0.10	184	Arain and Restrepo-Coupe (2005) and Peichl et al. (2010)
DBF	SK-OA	Boreal plains	53.62889	106.19779	3.8	1919	39	21	3.2	0.35	0.34±0.09	601	Barr et al. (2006)
GRL	AB-GRS	Prairies	49.70919	112.94025	0.88	–	6	0.365	4.6	0.25	0.26±0.10	951	Flanagan and Johnson (2005), Flanagan et al. (2002), Flanagan (2009) and Richardson et al. (2006)
MBF	ON-OMW	Boreal shield	48.21738	82.15553	3.0	1930	43.3	31.0	3.6	0.30	0.29±0.09	341	McCaughey et al. (2006)
WL	AB-WPL	Boreal plains	54.95384	112.46698	2.6	1958[c]	9	Tree: 3	2.0	0.15	0.20±0.04	626	Syed et al. (2006)
	ON-EPL	Mixed wood plains	45.40940	75.51870	1.4	–	3.0	Shrub: 0.25	2.3	0.10	0.09±0.05	70	Admiral and Lafleur (2007) and Peichl et al. (2010)

[a] *LAI*, T_e, h_m, h_c, u_*^{th}, u and H_e are leaf area index, established time, EC sensor height, canopy height, annual mean wind speed, friction velocity (u_*) threshold, and elevation above sea level, respectively. Values of h_m, h_c, u_*^{th} and u are for 2006; $u_*^{th}(EC)$ was determined by each tower operator (principal investigator) for EC flux calculation and was time-constant; $u_*^{th}(FP)$ was standardized threshold for footprint (FP) calculation and was time-varying; and $\mu\pm\sigma$ presents annual mean ±1 standard deviation.
[b] Vegetation types: CBF — Coniferous boreal forest, CMF — Coniferous maritime forest, CTF — Coniferous temperate forest, DBF — Deciduous boreal forest, GRL — Grassland, MBF — Mixed wood boreal forest, WL — Wetland.
[c] Site names: First two letters indicate the province (MB — Manitoba, QC — Quebec, SK — Saskatchewan, NB — New Brunswick, BC — British Columbia, ON — Ontario, AB — Alberta); NOBS — Northern Old Black Spruce, EOBS — Eastern Old Black Spruce, OJP — Old Jack Pine, SOBS — Southern Old Black Spruce, OBF — Old Balsam Fir, DF49 — Douglas fir (established 1949), WPP39 — White Pine Plantation (established 1939), OA — Old Aspen, GRS — grassland, OMW — Old mixed wood, WPL — Western peatland, EPL — Eastern peat land.

Atkinson, 1998; Şen, 1998; Sertel et al., 2007; Song and Woodcock, 2002; Woodcock et al., 1988). A semivariogram provides a concise and unbiased description of the scale and pattern of spatial variability and can be applied to spatial variability and autocorrelation in a region provided that the stationarity hypothesis is valid (Curran, 1988; Şen, 1998; Sertel et al., 2007). In this study, we used the semivariogram to estimate the spatial variation properties of vegetation, such as heterogeneity intensity, over the flux tower footprint area using a spectral index.

Table 2
Land cover classes of EOSD and aggregation schemes.

Site ID[a]		Vegetation function type[b]	Aggregated 8 types	EOSD classification scheme: 23 classes
MB-NOBS; SK-OJP; NB-OBF; ON-WPP39	QC-EOBS; SK-SOBS; BC-DF49;	CBF, CMF, CTF	Coniferous forest	Coniferous — dense; coniferous — open; coniferous — sparse
SK-OA		DBF	Broadleaf forest	Broadleaf — dense; broadleaf — open; broadleaf — sparse
ON-OMW		MBF	Mixed forest	Mixed wood — dense; mixed wood — open; mixed wood — sparse
AB-GRS		GRL	Grassland/ cropland	Herb (grasses, crops, forbs, and gramminoids)
AB-WPL; AB-WPL		WL	Wetland	Wetland — treed; wetland — shrub; wetland — herb
n/a		n/a	Shrub land	Shrub — tall; shrub — low
n/a		n/a	Water	Water
n/a		n/a	Others	Bryoids; exposed land; rock/rubble; snow/ice; shadow; cloud; no data

[a] See Table 1 for description of abbreviation of site name.
[b] See Table 1 for description of abbreviation of vegetation function type.

Considering a transect running across a remotely sensed vegetation index (z) image, the relation between any pair of pixels with h intervals apart (the lag distance) can be given by the squared difference between them. Therefore, the semivariance $\gamma(h)$ for paired pixels at distance h apart ($z(x)$ and $z(x+h)$), is defined following Curran (1988) as:

$$\gamma(h) = \frac{1}{2}E\left[\{z(x)-z(x+h)\}^2\right] \quad (1)$$

where E is the mathematical expectation operator and x is the pixel location.

The experimental (or sample) semivariogram for the $p(h)$ paired observations is estimated along a transect where $p(h)$ pairs of

Table 3
Acquired Landsat imagery information for CCP sites used in this study.

Vegetation type[a]	Site code[a]	Satellite	Dataset	Path	Row	Acquisition date
CBF	MB-NOBS	Landsat7	ETM+	034	021	2006/09/06
	QC-EOBS	Landsat5	TM	016	025	2002/08/28
	SK-OJP	Landsat7	ETM+	037	022	2006/08/26
	SK-SOBS	Landsat7	ETM+	037	022	2006/08/26
CMF	NB-OBF	Landsat7	ETM+	010	028	2005/08/26
CTF	BC-DF49	Landsat5	TM	049	025	2000/06/26
	ON-WPP39	Landsat5	TM	018	030	1999/09/03
DBF	SK-OA	Landsat5	TM	038	023	2001/08/03
GRL	AB-GRS	Landsat7	ETM+	041	025	2006/07/21
MBF	ON-OMW	Landsat5	TM	020	027	2002/09/09
WL	AB-WPL	Landsat5	TM	042	022	2001/08/15
	ON-EPL	Landsat7	ETM+	015	029	2005/09/14

[a] See Table 1 for description of abbreviation of site name.

observations separated by the same lag h, $\{z(x_i), z(x_i+h)\}, i = 1,2,\ldots,p(h)$,

$$\hat{\gamma}(h) = \frac{1}{2p(h)} \sum_{i=1}^{p(h)} \{z(x_i) - z(x_i+h)\}^2 \quad (2)$$

For remotely sensed imagery the lag (h) in Eq. (2) is measured in units of one side of a pixel (Berberoglu et al., 2007). The quantity $\hat{\gamma}(h)$ is an estimate of the semivariance of $\gamma(h)$ and is a useful measure of dissimilarity between spatially separate pixels and spatial patterns: the larger is the semivariance and the less similar are the pixels (Curran, 1988; Goovaerts, 1999; Sertel et al., 2007). The shape of the semivariogram reflects the spatial structure (Kim et al., 2006). A spherical model was used to fit the computed semivariogram and to estimate the coefficients of the model in this study. These parameters, such as *lag*, *sill*, *range*, and *nugget*, which are used to characterize the spatial variation properties, are illustrated in Fig. 2. In a typical semivariogram (Fig. 2), the semivariance values gradually increase with increasing lags and this diminishes with distance and levels off at a certain point. This distance at which the asymptote is reached is known as the *range*, signifying the extent of heterogeneity, at which spatial autocorrelation between data point pairs ceases, and beyond which data are stochastically independent (Ettenma & Wardle, 2002). The plateau of the semivariance estimates at the range value is the *sill*, which is a measure of total population variance, or absolute amount of heterogeneity (e.g. Cohen et al., 1990). The non-zero intercept of the semivariance curve with the y-axis is the *nugget*, indicating the non-spatial variation due to sampling error (Adams et al., 2008).

Twenty-four transects (with a 15° interval) were selected over the 90% annual footprint climatology area in 2006 for each of the individual sites. The NDVI of each 30-m pixel was used to calculate a semivariogram for each transect. An omnidirectional semivariogram was then estimated as the average of all directional transects.

2.6. Window size analysis

A simple window size analysis is also applied to assessing the landscape spatial homogeneity surrounding the individual towers at different scales based on NDVI coverage. The averaged values of vegetation index $\bar{\lambda}$ (i.e. NDVI) within a window (rectangle) of varying window size centered at the EC tower was plotted against the window width to see the variations of homogeneity with increasing spatial scales. The calculations were implemented by increasing the window size with distance ($\Delta r = 30$ m, 1 pixel) from tower location pixel. The serial of window widths are 30 m, $(1+i)\times 30$ m,..., 2970 m, where $i = 2, 4, \ldots, 98$.

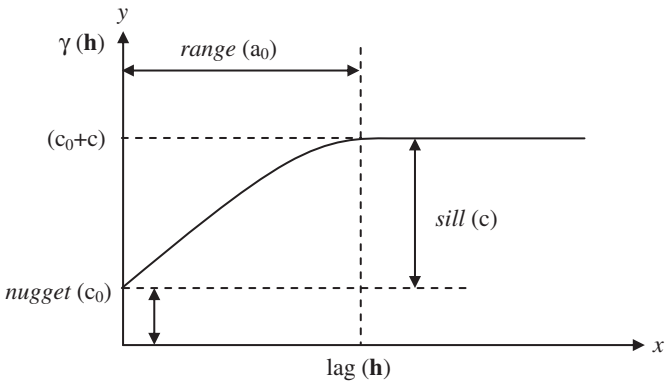

Fig. 2. Coefficients of a typical semivariogram model. The x axis shows the scale of variation, while the y axis shows the amount of variation.

3. Results

3.1. Footprint climatology

Fig. 3 shows the annual cumulative footprint climatology contours (50%, 80%, 90% and 99%) overlying the NDVI map at each study site. The NDVI variation illustrates the land surface heterogeneity within the footprint climatology area. For most sites, the annual footprint climatology was distributed asymmetrically around the tower. The annual footprint climatology area exponentially increased with increasing cumulative footprint percentage for all sites (Chen et al., 2011). The areas of 50%, 80%, 90% and 99% annual footprint climatology for the 12 sites are shown in Fig. 4. The sizes and orientations of annual footprint climatology were significantly different among the sites (Figs. 3 and 4). The annual footprint sizes of the two wetland sites (AB-WPL and ON-PEL) and the prairie land site (AB-GRS) were much smaller than those of the forested sites (Figs. 3 and 4) with the 90% annual footprint climatology less than 2.0 km^2. The areas of 90% annual footprint climatology for the nine forested land sites varied from 2.55 (NB-OBF) to 5.04 km^2 (SK-SOBS).

3.2. Land cover

Fig. 5 shows land cover maps overlain by the annual cumulative footprint climatology contours (50%, 80%, 90% and 99%) and Fig. 6 shows the frequency distribution of land cover types in the areas of 50%, 80%, 90% and 99% annual footprint climatologies for the 10 data-available sites using the land cover scheme (8 classes). Table 4 shows the percentages of the targeted vegetation functional type (dominant land cover type) using both land cover classification schemes (EOSD 23 types and aggregated 8 types) in the 50%, 80%, 90% and 99% annual footprint climatology areas and the circular areas centered at individual towers with radius of 1, 2, and 3 km. The percentage of EC tower observed target land cover using EOSD 23-type classification is much higher than using the aggregated 8-type classification for all sites (Table 4 and Fig. 6). The percentile of the dominant land cover type in the footprint climatology areas decreased with increasing cumulative footprint percentage and with increasing circular area's radius for most sites. A large decrease was found at one wetland site (AB-WPL), where the percentage dominant land cover of wetland-treed (23-type classification) or wetland (8-type classification) respectively decreased from 66% or 90% at 50% of annual footprint climatology to about 44% or 67 at 99% of annual footprint climatology (Fig. 6, Table 4). In terms of land cover distributions in the 99% footprint climatology area, the most homogeneous site was the BC-DF49 where the dominant land cover of coniferous forest accounted for about 95% of the annual footprint climatology area; whereas the two most heterogeneous sites were the SK-OA and ON-EPL sites. At the SK-OA site, the observed target land cover (broadleaf-dense forest in the EOSD 32-type classification scheme or broadleaf forest in the aggregated 8-type classification scheme) were about 30% or 40% respectively (Table 4). Mixed wood and coniferous forest accounted for about 30%–40% and around 20% in the 50% to 99% footprint climatology areas, respectively (Fig. 6). The old aspen stand at this site was about 87 years old in 2006 and showed a recessional trend. Errors in identification of broadleaf from mixed wood in the EOSD land cover products, which was derived from Landsat imagery, would also cause underestimating the percentage of observed target land cover of broadleaf forest. At the ON-EPL site, the areas of both wetland herb and wetland shrub accounted for about 30%–25% of the 50% to 99% annual footprint climatology areas (Table 4, Fig. 6). The target land cover of the ON-EPL tower is wetland and the combined wetland herb and shrub land cover accounted for about 60%–50% of the 50% to 99% annual footprint climatology areas. Overall, the percentage of the target vegetation functional type using the aggregated land cover classification scheme (Table 2) observed by the tower was higher than 60% for most CCP sites (Table 4, Fig. 6).

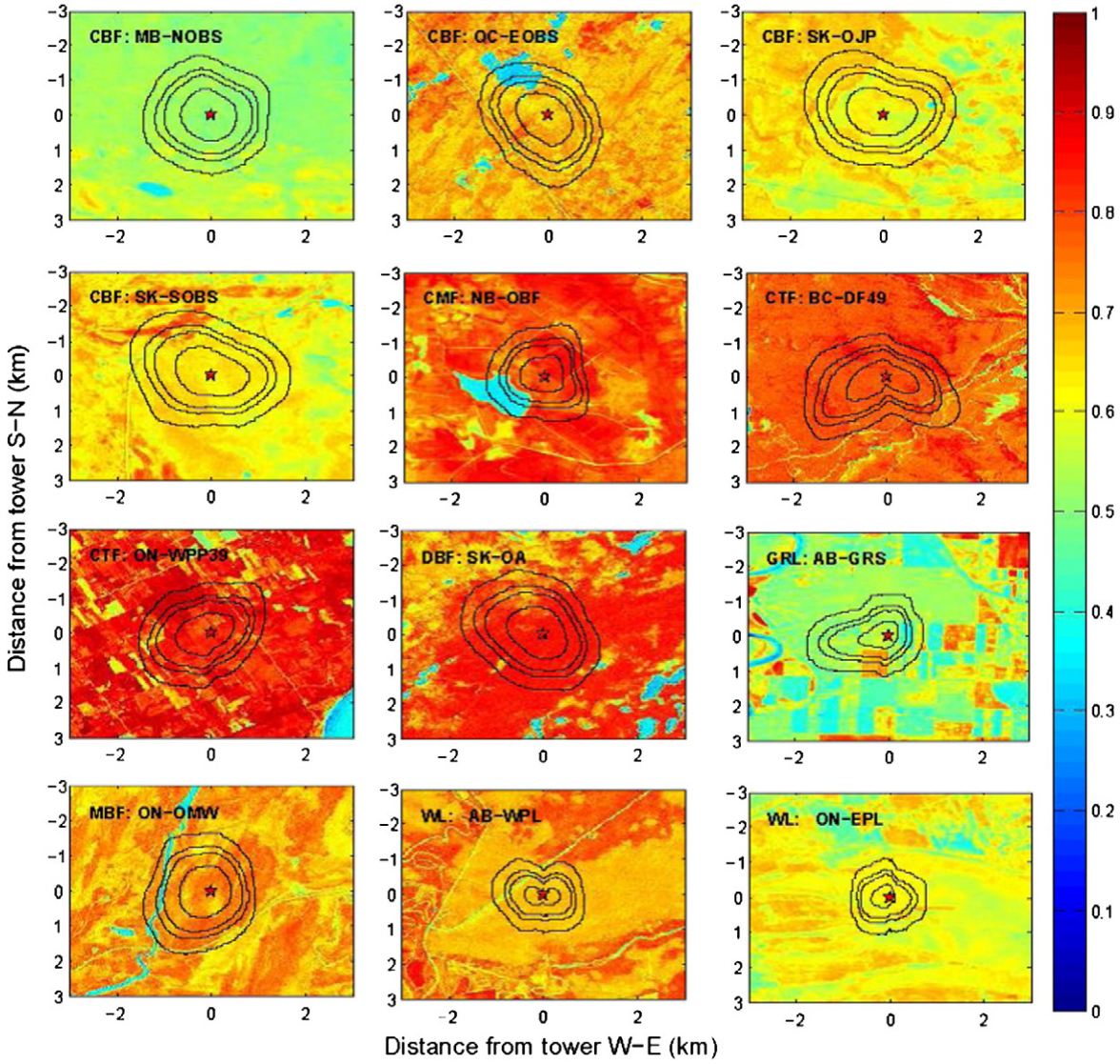

Fig. 3. NDVI (Normalized Difference Vegetation Index) maps at a 30-m resolution for each area (6×6 km) centered at individual CCP towers. The scene path and row and the acquisition dates are shown in Table 3. The contours from inner to outer are the 50%, 80%, 90% and 99% annual cumulative footprint climatology, respectively. For description of abbreviation of vegetation type and site name, see Table 1.

3.3. Semivariograms

Fig. 7 shows an omnidirectional semivariogram of NDVI of 90% annual footprint area for individual sites. The semivariogram shape of NDVI was different among these 12 sites, reflecting different spatial structure in the 90% annual footprint climatology area. The directional semivariograms of NDVI obtained along transects of 0–180°, 45–225°, 90–270° and 135–315° are shown in Fig. 8, for instance, to examine the dependency of the semivariogram on the direction. Most of the sites presented somewhat anisotropic characteristics of NDVI in the 90% annual footprint climatology area. The large land surface anisotropy sites were found to be AB-GRS, ON-OMW, SK-OJP and QC-EOBS. In addition, NB-OBF showed a typical semivariogram along the 135–315° transect, in which the semivariance curve dropped with increasing lags after reaching its summit (Fig. 8d). It is interesting that NDVI along the 135–315° transect presented higher heterogeneity than other directions for most sites. For instance, at the QC-EOBS site, the 135–315° transect crossed a lake to the northwest from the tower and wetland to the southeast from the tower (Fig. 5); at SK-OJP site the transect crossed wetland to the northwest from the tower (Fig. 5); at ON-OMW site, there is a river located along NE–SW to the west of the tower and most land cover types and other land surface characteristics distribute along this direction (Fig. 5), so it is easy to understand why the degree of NDVI heterogeneity derived from semivariogram along the 135–315° transect was higher than other directions.

The degree of heterogeneity (as measured by *sill*) of the flux footprint area differed among sites (Fig. 9). High *sill* values (high heterogeneity) were found at NB-OBF, ON-OMW and SK-OJP, while low *sill* values (less heterogeneity) were at BC-DF49, AB-WPL and ON-EPL (Fig. 9c). The spatial dependence can be measured by *range*. The coniferous boreal forest sites had comparatively high values of *range* (>500 m) whereas the two wetland sites and BC-DF49 had low values of *range* (<200 m) in the 50% through 99% footprint climatology areas (Fig. 9b), indicating the former had coarse spatial variability than the latter. The NDVI semivariograms for the sites did not pass through the origin and have *nugget* effects (Figs. 7–8), resulting from short-range spatial variation within pixels rather than between them (Atkinson, 1997; Sertel et al., 2007). Overall, the forest sites had relatively larger *nugget* values than the grassland and wetland sites (Fig. 9a), suggesting that the former had higher fine-scale spatial variability. For all sites, the degree of heterogeneity and the short-scale spatial variation increased with increasing size of the footprint climatology (Fig. 9a, c). The coarse spatial variation increased with increasing the size of the footprint climatology for most sites while three coniferous boreal forest sites

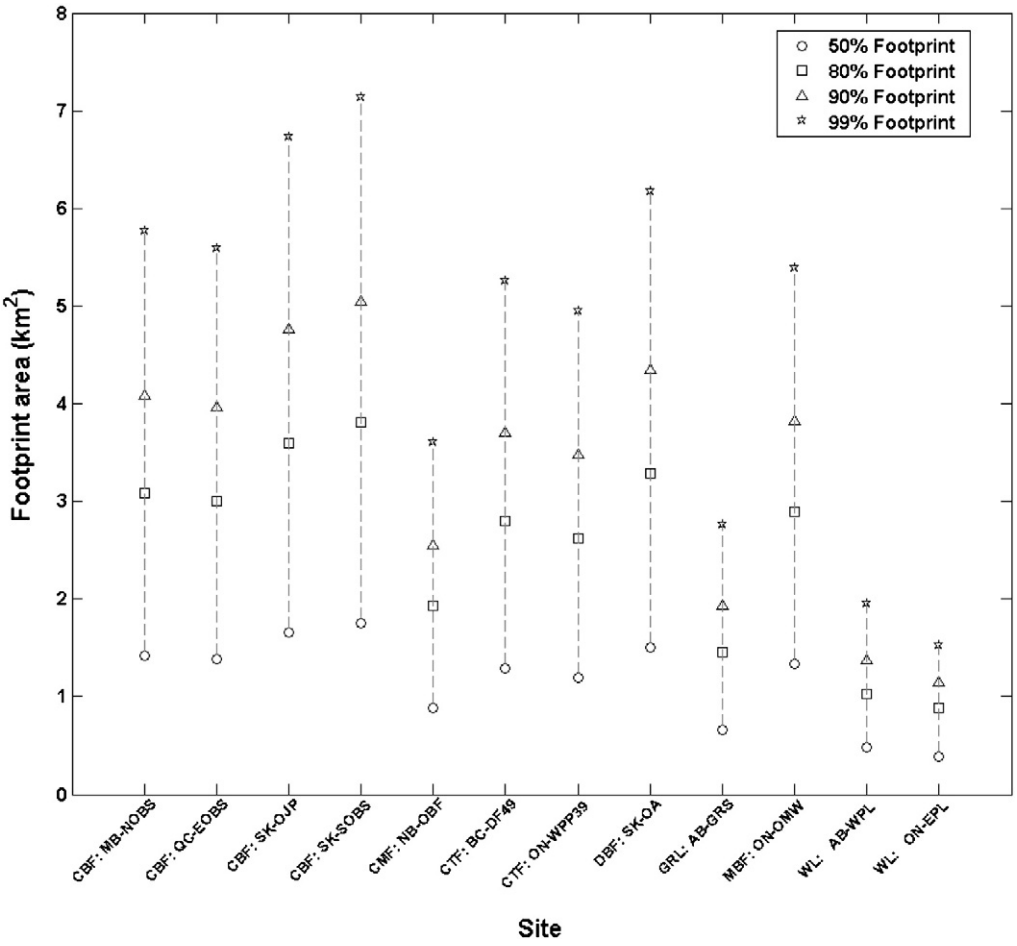

Fig. 4. Footprint areas of 50%, 80%, 90% and 99% annual footprint climatology for the twelve CCP sites in 2006. For description of abbreviation of vegetation type and site name, see Table 1.

(QC-EOBS, SK-OJP and SK-SOBS) showed high coarse spatial variation (high *range* value) in the 50% footprint climatology area (Fig. 9b).

3.4. Window size analysis

The representativeness of a specific flux tower location on the NDVI map can be assessed using a window size analysis (Fig. 10). The highest and lowest NDVI values were found at the SK-OA site and the MB-NOBS site with an average of 0.88 and 0.51, respectively. For most sites, the averaged NDVI value varied within a small range (<5%) with increasing window width up to 3 km, reflecting good representativeness of EC measurements across the CCP network. Exceptions include the following three sites: SK-OJP, ON-EPL and NB-OBF. For the SK-OJP site, the average NDVI increased from 0.55 to 0.65 at the window width of 0 to 1.3 km, and then remained constant with the window width from 1.3 up to 3 km (Fig. 10); whereas for the ON-EPL, the average NDVI decreased from 0.65 to 0.55 at the window width of 0 to 1.6 km, and remained constant with the window width from 1.6 up to 3 km (Fig. 10). The largest variation in average NDVI with varying window size was found at the NB-OBF site, reflecting higher heterogeneity, consistent with the high *sill* value (Figs. 7 and 9c). For the NB-OBF site, the average NDVI rapidly increased to 0.83 at the window width of 0.15 km, was steady at this value to the window width of 0.4 km decreased to 0.72 at the window width of 1.1 km, and then gradually increased up to the window width of 3 km. This drop of NDVI for the window width of 0.4 to 1.1 km is likely due to a lake southwest of the tower at this distance (Fig. 6, panel CMF: NB-OBF).

Fig. 10 indicates that the tower flux measurements at most of the CCP sites adequately represent NDVI over the 90% cumulative annual footprint climatology area. Caution should be paid to interpret/assess the tower measured fluxes at the three sites (NB-OBF, SK-OJP and ON-EPL) because at these sites, the measured fluxes are somewhat dependent on the wind direction and the footprint size. The results of the semivariogram and window size analysis suggest that the combination of these two techniques can be effectively used either to assess the pre-existing flux tower's spatial representativeness or to address scaling issue or to perform a priori optimization of an initial tower location. Moreover, directional analysis of semivariogram and window size for different wind sectors provides insightful information on tower sensor location bias in conjunction with the flux footprint climatology and wind climatology analysis.

4. Discussion

4.1. Limitations and uncertainties

Land surface characteristics, such as the type and density of vegetation cover, varies across a range of scales from a few millimeters to hundreds of kilometers (Anderson et al., 2003; Chehbouni et al., 2000; Mahrt et al., 2001), exert a critical control on the turbulent exchange of mass and energy at the land–atmosphere interface (Caparrini et al., 2004; Pielke et al., 1998; Weaver et al., 2002; Wilson & Baldocchi, 2000). Surface spatial heterogeneity has a strong impact on the observed surface fluxes (Kim et al., 2006; Yates et al., 2003), so an accurate representation of surface characteristics over an EC flux tower footprint area is important for understanding the measured land–atmosphere

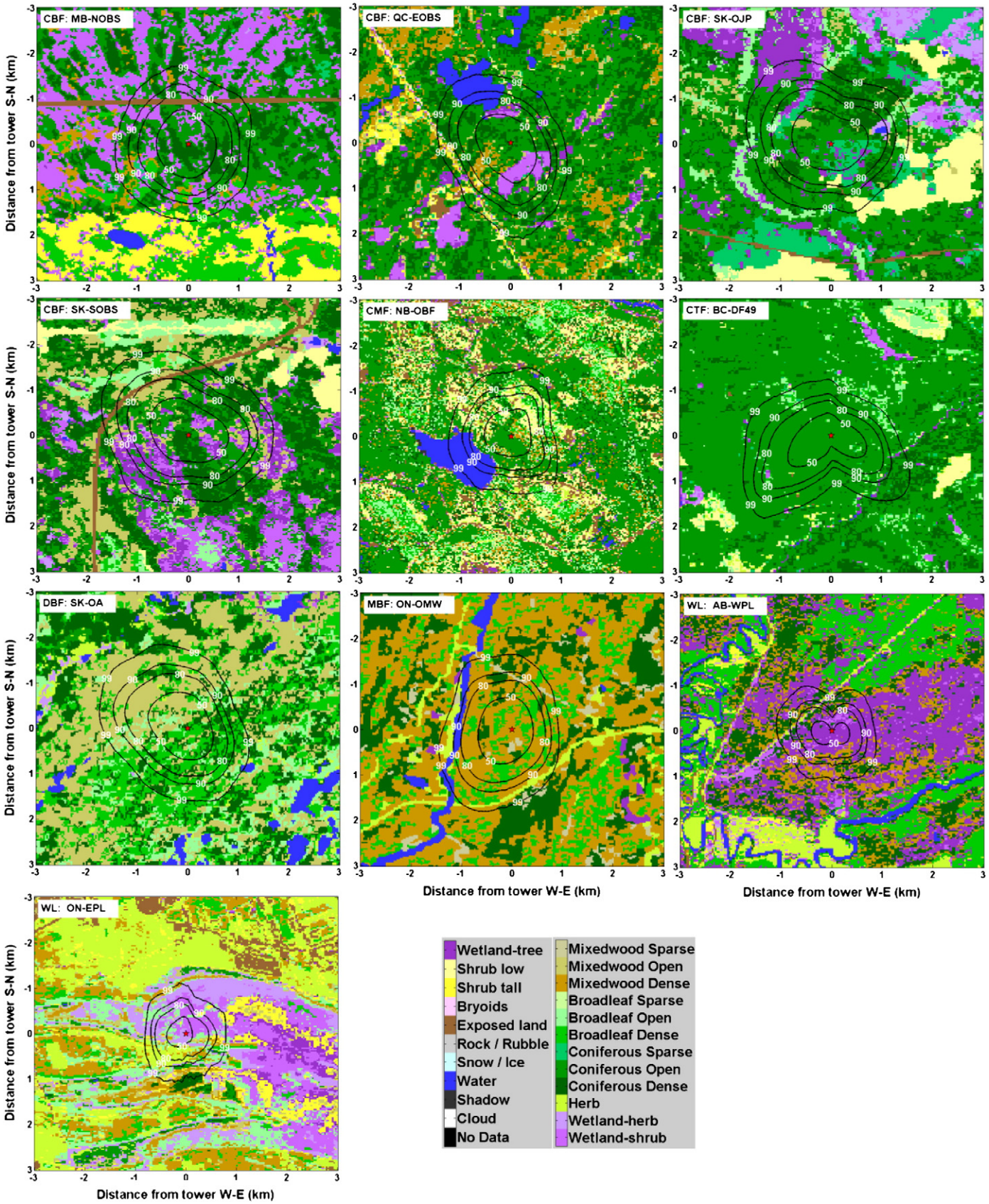

Fig. 5. Land cover maps of the ten data-available CCP sites at a 30-m resolution for each area (6×6 km) centered at individual CCP sites. The contours from inner to outer are the 50%, 80%, 90% and 99% annual cumulative footprint climatology, respectively. For description of abbreviation of vegetation type and site name, see Table 1.

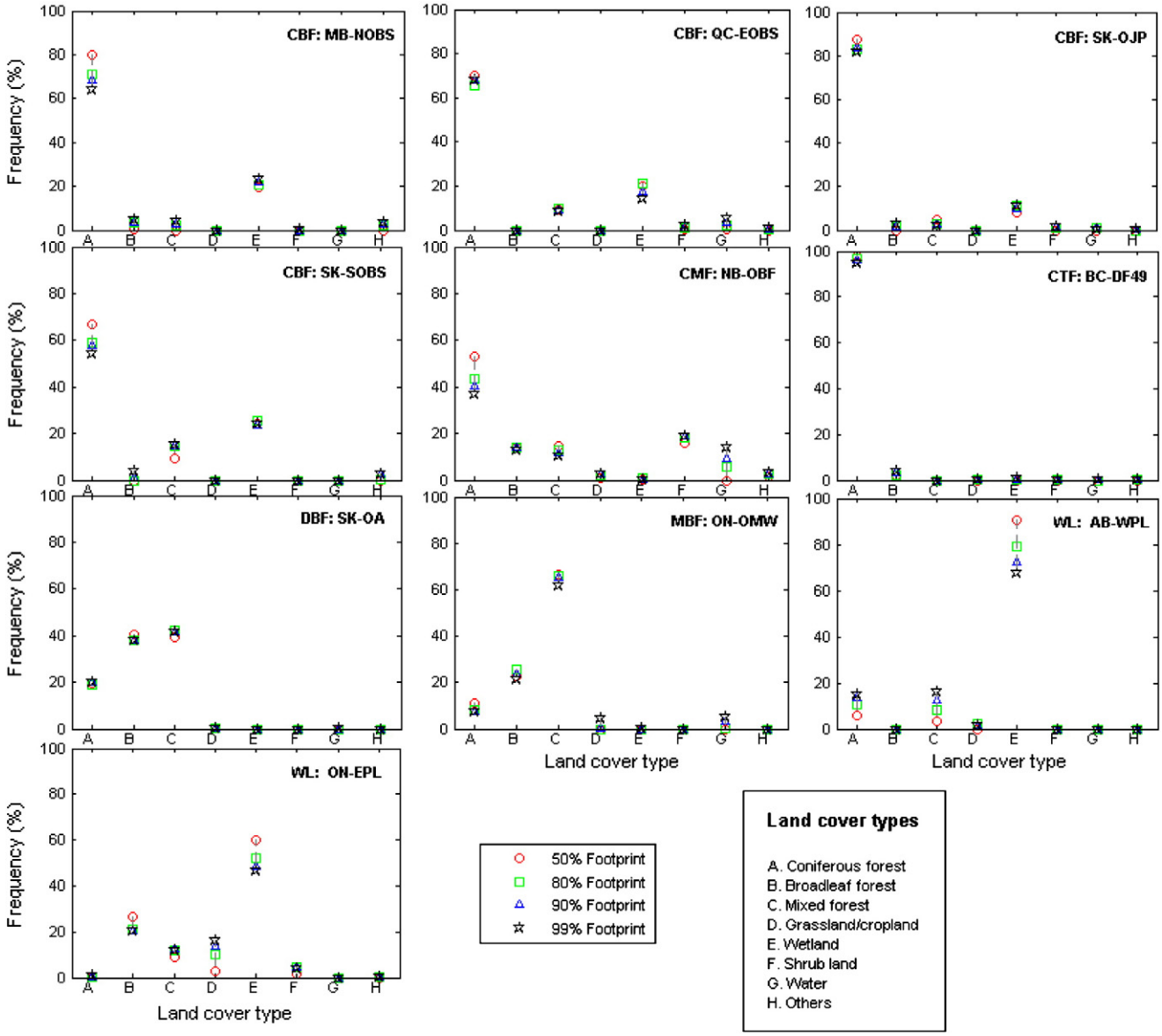

Fig. 6. Frequency distribution of land cover types for the ten data-available CCP sites in the areas of 50%, 80%, 90% and 99% annual footprint climatologies. For description of abbreviation of vegetation type and site name, see Table 1.

exchange processes (Alfieri, 2009; Kalma et al., 2001). Reliable footprint climatologies in conjunction with detailed land cover classification, and remotely sensed vegetation indices can be used to fully characterize the spatial variation of heterogeneous landscapes and to assess the quality of the annual and long-term EC flux measurements.

The semivariogram and window size analysis based solely on Landsat data provides important information on the structure, amount and extent of spatial heterogeneity of land surface vegetation surrounding the flux tower. The results of semivariogram and window size analysis are consistent with sensor location bias (SLB) estimates based on footprint modeling (Chen et al., 2011) and are helpful for understanding the latter results. The combination of footprint modeling, semivariogram and window size techniques, together with remotely-sensed image data (land cover products and vegetation indices) at a fine-resolution (e.g. 30 m at this study or less), is a pragmatic approach for assessing the spatial representativeness flux tower measurements.

Errors in land cover and vegetation indices and biases in footprint climatology estimates will lead to uncertainty in EC flux tower's spatial representativeness assessment. The SAFE-F footprint model used in this study applies to most conditions of atmospheric stability using a stationary gradient diffusion formulation with height-independent crosswind dispersion. Model comparison showed that the overall biases of SAFE-F are within 5% of other state-of-the-art footprint models (Chen et al., 2011). It is important to keep in mind that land surface heterogeneity (e.g. trees, shrubs) and other topographic elements influence the wind flow, e.g. creating internal boundary layers (Stull, 1988). The applied analysis footprint model (e.g. SAFE-F) is unable to account for such effects, thus the spatial representativeness assessments are subject to footprint model uncertainty.

The EC flux footprint climatology was also found to significantly vary with the different flux components (Chen et al., 2009a). In order to confirm their findings and compare the differences in SLB estimation between using different indices, Chen et al. (2011) used both NDVI and enhanced vegetation index (EVI) as surrogates of land surface source strength and found that the difference in estimated SBL between NDVI and EVI for most CCP sites was not significant with exception of ON-OMW and SK-OJP (Chen et al., 2011). In this sense, using NDVI as a flux surrogate in this study is only a first-order estimate because of its limitations, such as under saturation condition, it is not sensitive to changes in green biomass amount and variations in vegetation functions. In addition, given large seasonal variations of carbon and water fluxes and the single satellite image (one image for the whole year in

Table 4
Percentages of observed dominant land cover type in a reference footprint area: 50%, 80%, 90% and 99% annual footprint climatology areas and the circular areas centered at each tower location with radius of 1, 2, and 3 km.

Vegetation type ID[a]	Site ID[b]	Overstory vegetation species	Observed dominant land cover type[c]	Reference land surface area						
				Footprint climatology area of				Circular area centered at individual towers with radius of		
				50%	80%	90%	99%	1 km	2 km	3 km
CBF	MB-NOBS	*Picea mariana*	Coniferous — open	45.55	43.11	42.42	41.66	45.89	38.56	32.14
			Coniferous forest	**80.10**	**71.06**	**68.69**	**64.14**	**74.53**	**56.23**	**46.47**
	QC-EOBS	*Picea mariana*	Coniferous — open	48.47	44.52	44.33	43.54	44.94	47.60	47.79
			Coniferous forest	**69.88**	**65.36**	**67.86**	**67.82**	**66.87**	**69.92**	**69.12**
	SK-OJP	*Pinus banksiana*	Coniferous — open	54.62	45.68	48.46	50.60	49.61	45.55	40.57
			Coniferous forest	**87.43**	**82.83**	**83.53**	**81.97**	**86.69**	**72.82**	**62.28**
	SK-SOBS	*Picea mariana*	Coniferous — open	41.08	38.70	36.12	32.71	38.86	30.28	25.73
			Coniferous forest	**66.62**	**59.13**	**57.74**	**54.23**	**66.30**	**54.72**	**50.44**
CMF	NB-OBF	*Abies balsamea*	Coniferous — open	41.90	34.87	31.79	28.41	27.74	36.28	37.12
			Coniferous forest	**52.94**	**43.65**	**40.13**	**37.10**	**36.76**	**45.68**	**47.21**
CTF	BC-DF49	*Pseudotsuga menziesii*	Coniferous — open	96.32	95.57	94.09	90.24	94.53	83.81	79.39
			Coniferous forest	**98.05**	**96.88**	**96.14**	**94.85**	**96.37**	**90.86**	**88.72**
	ON-WPP39	*Pinus strobus L.*	–	–	–	–	–	–	–	–
DBF	SK-OA	*Populus tremuloides*	Broadleaf — dense	29.00	29.07	29.33	29.90	33.97	30.41	24.00
			Broadleaf forest	**40.56**	**38.26**	**37.83**	**38.11**	**43.96**	**39.20**	**34.00**
GRL	AB-GRS	–		–	–	–	–	–	–	–
MBF	ON-OMW	*Populus tremuloides*, *Picea mariana*, *Picea glauca*,*Betula papyrifera* *Abies balsamea*	Mixed wood — dense	61.90	63.75	63.06	58.59	62.66	51.69	51.07
			Mixed wood forest	**66.47**	**65.86**	**65.07**	**61.47**	**64.62**	**55.51**	**54.57**
WL	AB-WPL	*Larix laricina*, *Picea mariana*	Wetland — treed	66.49	51.70	46.25	44.11	52.09	41.98	30.23
			Wetland	**90.57**	**79.08**	**72.19**	**67.28**	**59.55**	**47.72**	**34.68**
	ON-EPL	–	Wetland — herb	26.41	23.43	24.34	23.65	25.27	17.45	12.81
			Wetland	**59.95**	**52.25**	**48.78**	**46.77**	**45.84**	**31.86**	**24.34**

[a] See Table 1 for description of abbreviation of site name.
[b] See Table 1 for description of abbreviation of vegetation function type.
[c] Land cover classes of EOSD (23 types) and aggregation schemes (8 types, bold fonts), see Table 2 for detail.

this study), the uncertainty in the land surface spatial characterization is worth considering. Landsat imagery at a 30-m spatial resolution is well suited for characterizing landscape-level forest structure and is ideal for characterizing flux tower's spatial representativeness. Its 16-day revisit-cycle, is however, generally lengthened by frequent cloud contamination and other poor atmospheric conditions (Ju & Roy, 2007). At the CCP sites, for instance, there are a very limited number of scenes available in, or close to, 2006, which is ultimately insufficient for studying the seasonality of vegetation dynamics. The imagery data used in this study was acquired for each site during the growing season across a range of years (1999–2006; Table 3). Kim et al. (2006) undertook a footprint analysis based on single remotely-sensed image-derived NDVI over an extended period by assuming that seasonal variation in NDVI affected all areas within the 6×6 km domain proportionally, with a similar phenological development for individual sites. Similarly, we can easily extend the assumption that the relative variability in observed NDVI does not change across years. As a result, we deemed this appropriates as the analysis was focused on the annual relative variability of NDVI. Under these assumptions we believe our analysis using the available NDVI data (Table 3) is useful.

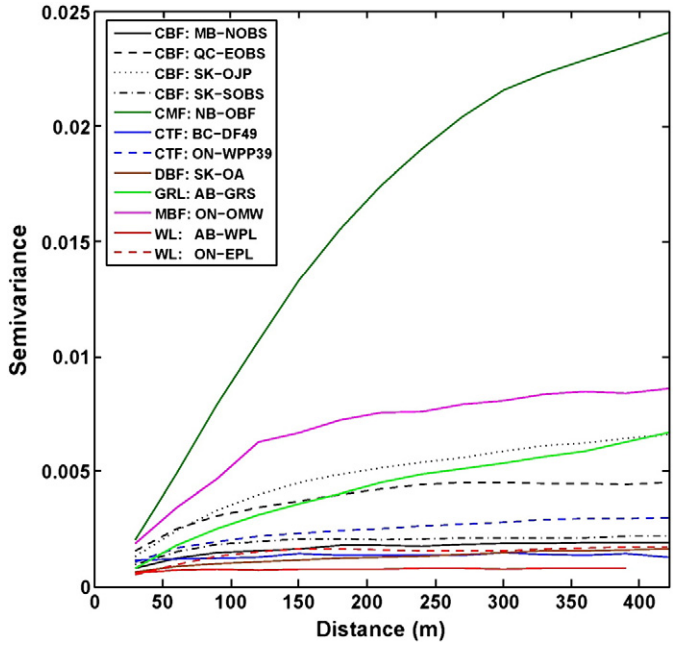

Fig. 7. Omnidirectional semivariogram of NDVI over the 90% annual footprint climatology area for individual CCP sites. For description of abbreviation of vegetation type and site name, see Table 1.

4.2. Implications

Proliferation of the FLUXNET database (www.fluxdata.org) offers unprecedented opportunities to study the dynamics of the terrestrial carbon and water cycles. However, this compilation does not provide spatially and temporally explicit maps of biosphere–atmosphere fluxes (Jung et al., 2009), but only the irregular distributed data points. In order to upscale the EC based land surface fluxes to large regions either using models or remote sensing measurements (e.g. Earth observation data), it is first necessary to correctly describe the surface heterogeneity over the flux tower footprint area. Satellite-borne remote sensing offers opportunities to parameterize vegetation characteristics of large spatial extent on variable spatial and temporal resolutions (Chen et al., 2009a). The remotely sensed data with variable spatial and temporal resolutions, however, require appropriate methods for upscaling and interfacing EC measurements to satellite observations (Drolet et al., 2005, 2008; Hall et al., 2008). The EC flux tower's footprint generally varies depending on wind speed, wind direction and atmospheric stability (Chen et al., 2009a); whereas the remotely sensed imagery data have fixed footprint (image pixel size) at different resolutions. The EC flux

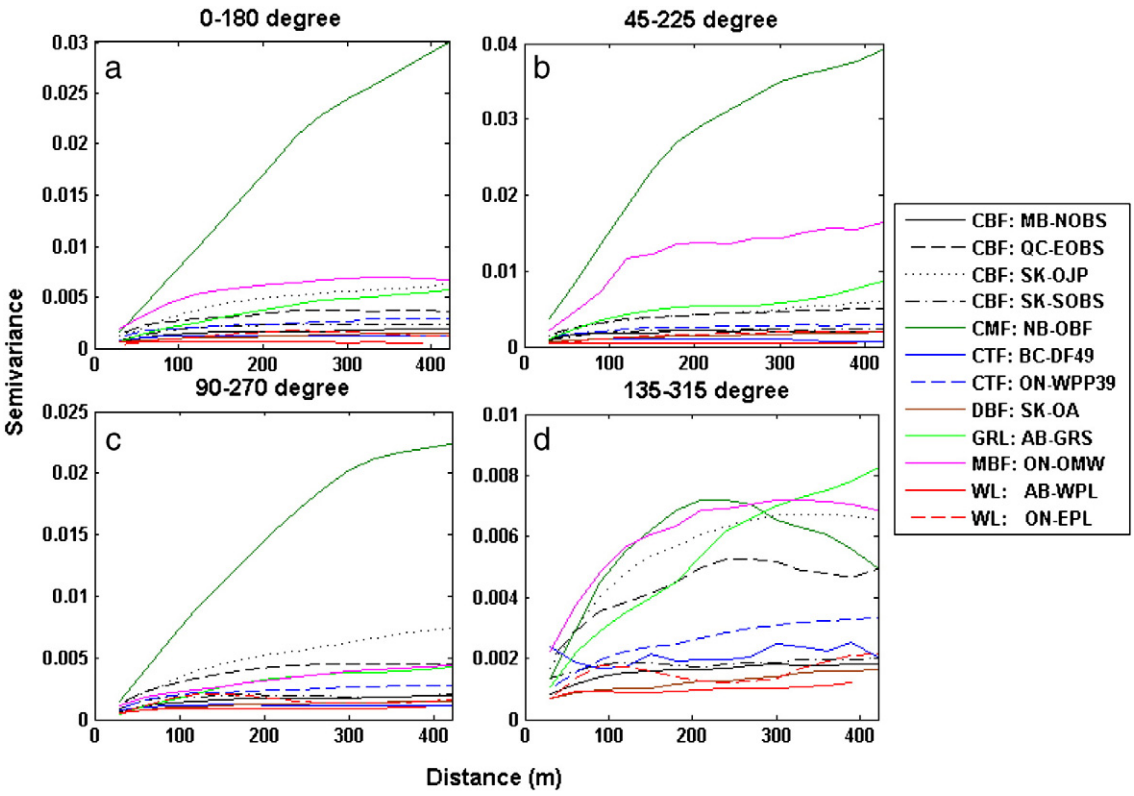

Fig. 8. Directional semivariograms of NDVI over the 90% annual footprint climatology area. For description of abbreviation of vegetation type and site name, see Table 1.

tower's footprint generally does not match the satellite pixel size (Chen et al., 2009a). Jung et al. (2008) employed measures of similarity between the 1×1 km and 3×3 km FAPAR (fraction of absorbed photosynthetic active radiation) time series at the sites to assess the degree of local landscape heterogeneity and found that large heterogeneity makes it likely that the smaller footprint of the flux tower is not representative for the area sampled by the satellite pixels (i.e. the scale mismatch between the tower and satellite footprint), and such sites should not be included in extrapolation. Jung et al. (2009) further concluded that the distinction between inter- and extrapolation can be more fuzzy without the information on flux tower's spatial representativeness to determine what controls structural similarity. Yang et al. (2007) used statistical and machine learning methods to extrapolate tower-based GPP (gross primary productivity) to a regional to continental scale for the U.S.A. by simply choosing a 7×7 km region as the spatial representativeness for each flux site. The authors noticed that such an implication ignored land surface heterogeneity over the EC flux footprint area and at the landscape scale could lead to inadequate representation of the nonlinearity of vegetation photosynthesis and respiration processes, and consequently their up-scaled results are likely to be somewhat in error. The findings in this study and by others (Chen et al., 2009a, 2011; Jung et al., 2009; Yang et al., 2007) suggested that ignoring land surface heterogeneity in the EC flux footprint area at the landscape scale could lead to inadequate representation of the nonlinearity of vegetation photosynthesis and respiration processes, and consequently the up-scaled results are likely to be in error.

4.3. Applications and future directions

Most of the FLUXNET sites are operated in more or less homogeneous environments (Barcza et al., 2009). Small-scale heterogeneity causes problems in ecosystem-scale EC measurements and they are considered as SLB (Chen et al., 2011). There are also a few EC flux towers that are located in regions with strongly heterogeneous land cover (Barcza et al., 2009). In cases of complex land cover spatial heterogeneity which leads to no dominant vegetation functional type, those data cannot be appropriately interpreted and attributed to plant functional types (Soegaard et al., 2003). Those data should be screened out in up-scaling approaches. Vegetation functional type specific data selection can be performed in the future with the synergy of footprint climatology analysis and a vegetation functional type map. Based on the presented approach, one may set up a criterion, such as the percentage of the dominant vegetation functional type observed by the EC tower in the 90% footprint climatology area, to screen the FLUXNET data. For instance, the percentage can be 50% or 60% according to the research objective or expected accuracy of up-scaled regional or global land surface fluxes (carbon, water or heat). We may obtain more detailed information on spatial representativeness of EC flux tower measurements by using semivariogram and window size techniques, together with remotely-sensed imagery data. Using selected vegetation functional types specific EC data with their quantitative representativeness information, it will be possible to inverse/derive biome (vegetation functional type) specific parameters for light-use-efficiency models or processed-based biogeochemical models (e.g. Chen et al., 2007a, b) using data-model assimilation techniques. Furthermore, with this information, the global available FLUXNET dataset may be used for the calibration and validation of remotely-sensed products such as the net photosynthesis product of the MODIS sensor (MOD17, Running et al., 1999).

The complexity and large computation demand of some footprint models restricts their practical applicability to global EC database. This is only feasible/applicable if the model is somewhat simplified, e.g. SAFE-F, which is based on an approximate analytical solution of the diffusion–advection equation. The SAFE-F model is suitable for global application.

In addition, to keep the overall site evaluation approach practical and widely applicable, the remotely sensed data sources have to be commercially available and low-cost, and must provide suitable spatial and spectral characteristics. As shown in this study, thus, the multi-spectral satellite data of Landsat (ETM and ETM+) at a 30-m spatial resolution are adequate to global FLUXNET application.

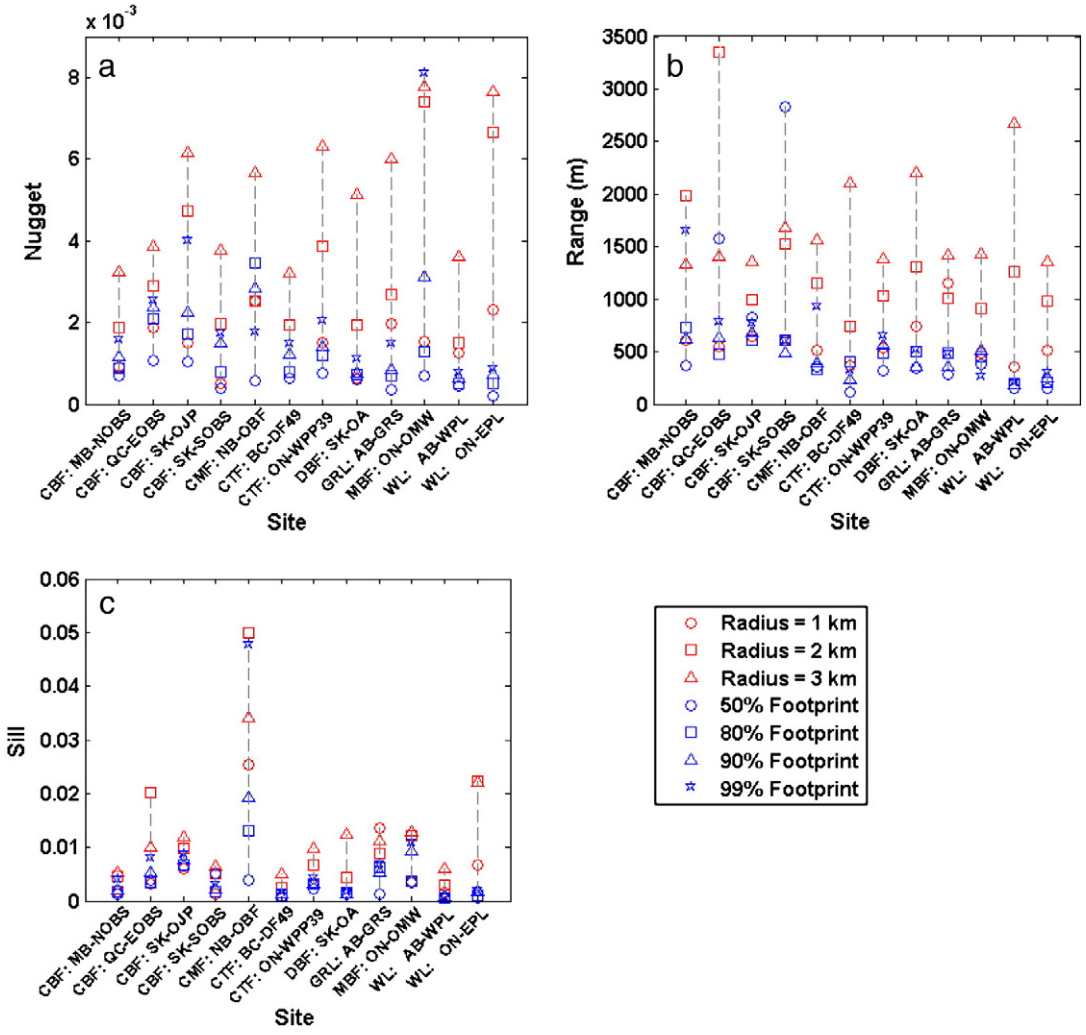

Fig. 9. Omnidirectional semivariogram parameters of NDVI over the areas of 50%, 80%, 90% and 99% annual footprint climatologies and the circular areas centered at individual towers with radius of 1, 2, and 3 km. For description of abbreviation of vegetation type and site name, see Table 1.

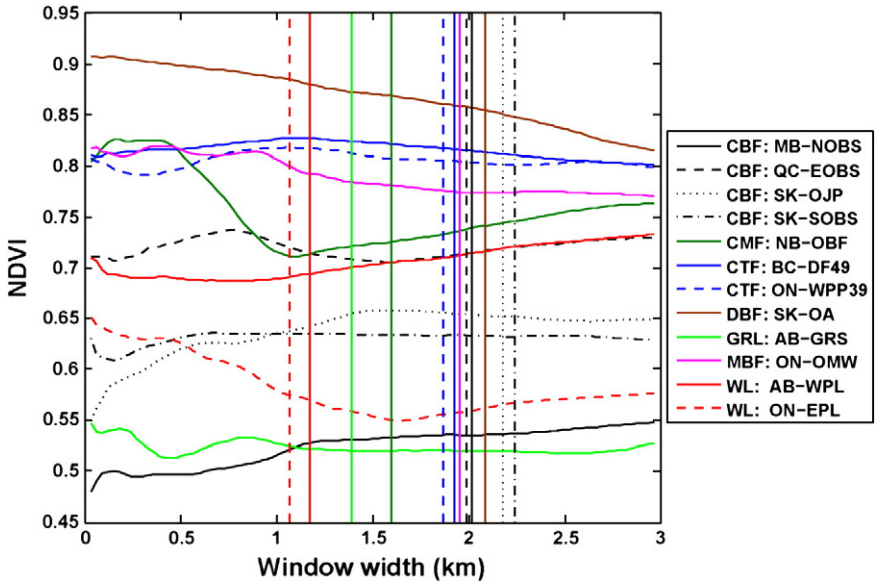

Fig. 10. The window-averaged NDVI of varying size with the tower location at the center of the window. Vertical lines show the window width (d) matching the 90% annual footprint climatology area (A_{90}), where $d = \sqrt{A_{90}}$. For description of abbreviation of vegetation type and site name, see Table 1.

5. Conclusions

The spatial representativeness of the main 12 CCP flux towers was evaluated by examining the spatial structure of the detailed land cover classification and remotely sensed vegetation indices at 30-m resolution over the modeled footprint areas. The following conclusions are drawn:

(i) The percentage of the target vegetation type observed by the EC tower in the 50% to 99% footprint climatology areas was higher than 60% for most CCP sites (Table 4). In terms of land cover distributions in the 99% footprint climatology area, the most homogeneous site was the BC-DF49 where the dominant land cover of coniferous forest accounted for about 95% of the annual footprint climatology area; whereas the two most heterogeneous were the SK-OA and ON-EPL sites.

(ii) Most of the CCP sites presented somewhat anisotropically distributed patterns of NDVI within the 90% annual footprint climatology area. The sites with the greatest anisotropy were found to be AB-GRS, ON-OMW, SK-OJP and QC-EOBS. The degree of land surface heterogeneity over flux footprint area differed among the sites: NB-OBF, ON-OMW and SK-OJP had comparatively high heterogeneity density while BC-DF49, AB-WPL and ON-EPL had comparatively low heterogeneity density. The coniferous boreal forest sites had higher coarse spatial variability than the two wetland and one coniferous temperate forest site (BC-DF49). Overall, the forest sites had larger fine-scale spatial variation than the grassland and wetland sites.

(iii) The presented approach for evaluating the spatial representativeness of the CCP flux network could be applied to the global network of EC towers (FLUXNET). If the spatial representativeness of the FLUXNET towers are evaluated using a remote sensing approach with the synergy of footprint climatology analysis and vegetation functional type map at 30-m resolution, and the land surface heterogeneity is explicitly taken into account using semivariogram and remotely-sensed imagery data, the estimations of regional and global fluxes will be improved.

Acknowledgments

This research is supported by a research grant (2010CB950704) under the Global Change Program of the Chinese Ministry of Science and Technology, a research grant (41071059) funded by the National Science Foundation of China, “One hundred talents” program funded by Chinese Academy of Sciences, an Alexander Graham Bell Canada Scholarship (CGS) funded by the Natural Sciences and Engineering Research Council of Canada (NSERC), the Canadian Carbon Program also funded by NSERC. Contributions from the many researchers involved in data collection and in-kind support from many government and private agencies for each study site are also gratefully acknowledged. Three anonymous reviewers and Dr. Scott Goetz (Associate Editor) provided constructive comments that greatly improved this paper.

References

Adams, C. F., Harris, B. P., & Stokesbury, K. D. E. (2008). Geostatistical comparison of two independent video surveys of sea scallop abundance in the Elephant Trunk Closed Area, USA. *ICES Journal of Marine Science: Journal du Conseil*, *65*, 995–1003.

Admiral, S. W., & Lafleur, P. M. (2007). Modelling of latent heat partitioning at a bog peatland. *Agricultural and Forest Meteorology*, *144*, 213–229.

Alfieri, J.G. (2009). Impacts of spatial heterogeneity of the measurement and modeling of land–atmosphere interactions. Doctorial Dissertation, Purdue University, West Lafayette, Indiana.

Anderson, M. C., Kustas, W. P., & Norman, J. M. (2003). Upscaling and downscaling — A regional view of the soil–plant–atmosphere continuum. *Agronomy Journal*, *95*, 1408–1423.

Arain, M. A., & Restrepo-Coupe, N. (2005). Net ecosystem production in a temperate pine plantation in southeastern Canada. *Agricultural and Forest Meteorology*, *128*, 223–241.

Atkinson, P. M. (1997). On estimating measurement error in remotely-sensed images with the variogram. *International Journal of Remote Sensing*, *18*, 3075–3084.

Atkinson, P. M., & Lewis, P. (2000). Geostatistical classification for remote sensing: an introduction. *Computers & Geosciences*, *26*, 361–371.

Baldocchi, D. D. (2003). Assessing the eddy covariance technique for evaluating carbon dioxide exchange rates of ecosystems: Past, present and future. *Global Change Biology*, *9*, 479–492.

Baldocchi, D. D. (2008). Breathing of the terrestrial biosphere: Lessons learned from a global network of carbon dioxide flux measurement systems. *Australian Journal of Botany*, *56*, 1–26.

Barcza, Z., Kern, A., Haszpra, L., & Kljun, N. (2009). Spatial representativeness of tall tower eddy covariance measurements using remote sensing and footprint analysis. *Agricultural and Forest Meteorology*, *149*, 795–807.

Barr, A. G., Morgenstern, K., Black, T. A., McCaughey, J. H., & Nesic, Z. (2006). Surface energy balance closure by the eddy-covariance method above three boreal forest stands and implications for the measurement of the CO_2 flux. *Agricultural and Forest Meteorology*, *140*, 322–337.

Berberoglu, S., Lloyd, C. D., Atkinson, P. M., & Curran, P. J. (2000). The integration of spectral and textural information using neural networks for land cover mapping in the Mediterranean. *Computers & Geosciences*, *26*, 385–396.

Berberoglu, S., Curran, P. J., Lloyd, C. D., & Atkinson, P. M. (2007). Texture classification of Mediterranean land cover. *International Journal of Applied Earth Observation and Geoinformation*, *9*, 322–334.

Black, T. A., Chen, W. J., Barr, A. G., Arain, M. A., Chen, Z., & Nesic, Z. (2000). Increased carbon sequestration by a boreal deciduous forest in years with a warm spring. *Geophysical Research Letters*, *27*, 1271–1274.

Caparrini, F., Castelli, F., & Entekhabi, D. (2004). Estimation of surface turbulent fluxes through assimilation of radiometric surface temperature sequences. *Journal of Hydrometeorology*, *5*, 145–158.

Chehbouni, A., Watts, C., Kerr, Y. H., Dedieu, G., Rodriguez, J. C., Santiago, F., Cayrol, P., Boulet, G., & Goodrich, D. C. (2000). Methods to aggregate turbulent fluxes over heterogeneous surface: Application to SALSA data set in Mexico. *Agricultural and Forest Meteorology*, *105*, 133–144.

Chen, B., Black, A., Coops, N. C., Hilker, T., Trofymow, T., Nesic, Z., & Morgenstern, K. (2009a). Assessing tower flux footprint climatology and scaling between remotely sensed and eddy covariance measurements. *Boundary-Layer Meteorology*, *130*, 137–167.

Chen, B., Black, A., Coops, N. C., Jassal, R., & Nesic, Z. (2009b). Seasonal controls on interannual variability in carbon dioxide exchange of a Pacific Northwest Douglas-fir forest, 1997–2006. *Global Change Biology*, *15*, 1962–1981.

Chen, B., Chen, J. M., & Ju, W. (2007a). Remote sensing based ecosystem–atmosphere simulation Scheme (EASS) — Model formulation and test with multiple-year data. *Ecological Modeling*, *209*, 277–300.

Chen, B., Chen, J. M., Mo, G., Yuen, C. -W., Margolis, H., Higuchi, K., & Chan, D. (2007b). Modeling and scaling coupled energy, water, and carbon fluxes based on remote sensing: An application to Canada's landmass. *Journal of Hydrometeorology*, *8*, 123–143.

Chen, B., Coops, N. C., Fu, D., Margolis, H. A., Amiro, B. D., Barr, A. G., Black, T. A., Arain, M. A., Bourque, C. P. -A., Flanagan, L. B., Lafleur, P. M., McCaughey, J. H., & Wofsy, S. C. (2011). Assessing eddy-covariance flux tower location bias across the Fluxnet-Canada Research Network based on remote sensing and footprint modeling. *Agriculture and Forest Meteorology*, *150*, 87–100.

Cohen, W. B., Spies, T. A., & Bradshaw, G. A. (1990). Semivariograms of digital imagery for analysis of conifer canopy structure. *Remote Sens. Environ.*, *34*, 167–178.

Curran, P. J. (1988). The semivariogram in remote sensing: An introduction. *Remote Sensing of Environment*, *24*, 493–507.

Curran, P. J., & Atkinson, P. M. (1998). Geostatistics and remote sensing. *Progress in Physical Geography*, *22*, 61–78.

Drolet, G. G., Huemmrich, K. F., Hall, F. G., Middleton, E. M., Black, T. A., Barr, A. G., et al. (2005). A MODIS-derived photochemical reflectance index to detect inter-annual variations in the photosynthetic light-use efficiency of a boreal deciduous forest. *Remote Sensing of Environment*, *98*, 212–224.

Drolet, G. G., Middleton, E. M., Huemmrich, K. F., Hall, F. G., Amiro, B. D., Barr, A. G., et al. (2008). Regional mapping of gross light-use efficiency using MODIS spectral indices. *Remote Sensing of Environment*, *112*, 3064–3078.

Dunn, A., Barford, C. C., Wofsy, S., Goulden, M. L., & Daube, B. C. (2007). A long-term record of carbon exchange in a boreal black spruce forest: Means, responses to interannual variability and decadal trends. *Global Change Biology*, *12*, 1–14.

Ettenma, C., & Wardle, D. A. (2002). Spatial soil ecology. *Trends in Ecology & Evolution*, *17*, 177–183.

Field, C. B., Randerson, J. T., & Malmstrom, C. M. (1995). Global net primary production-combining ecology and remote sensing. *Remote Sensing of Environment*, *51*, 74–88.

Finnigan, J. J., Clement, R., Malhi, Y., Leuning, R., & Cleugh, H. A. (2003). A reevaluation of long-term flux measurement techniques Part I: Averaging and coordinate rotation. *Boundary-Layer Meteorology*, *107*, 1–48.

Flanagan, L. B. (2009). Phenology of plant production in the northwestern great plains: Relationships with carbon isotope discrimination, net ecosystem productivity and ecosystem respiration. In A. Noormets (Ed.), *Phenology of ecosystem processes* (pp. 169–185). New York: Springer Science, Business Media.

Flanagan, L. B., & Johnson, B. G. (2005). Interacting effects of temperature, soil moisture and plant biomass production on ecosystem respiration in a northern temperate grassland. *Agricultural and Forest Meteorology*, *130*, 237–253.

Flanagan, L. B., Wever, L. A., & Carlson, P. J. (2002). Seasonal and interannual variation in carbon dioxide exchange and carbon balance in a northern temperate grassland. *Global Change Biology*, *8*, 599–615.

Foken, T., & Wichura, B. (1996). Tools for quality assessment of surface-based flux measurements. *Agricultural and Forest Meteorology*, *78*, 83–105.

Franklin, S. E., & Wulder, M. A. (2002). Remote sensing methods in large area land cover classification using satellite data. *Progress in Physical Geography*, *26*, 173–205.
Gockede, M., Rebmann, C., & Foken, T. (2004). A combination of quality assessment tools for eddy covariance measurements with footprint modelling for the characterisation of complex sites. *Agricultural and Forest Meteorology*, *127*, 175–188.
Goovaerts, P. (1999). Geostatistics in soil science: state-of-the-art and perspectives. *Geoderma*, *89*, 1–45.
Goulden, M. L., Munger, J. W., Fan, S. M., Daube, B. C., & Wofsy, S. C. (1996). Measurements of carbon sequestration by long-term eddy covariance: Methods and a critical evaluation of accuracy. *Global Change Biology*, *2*, 169–182.
Govind, A., Chen, J. M., & Ju, W. (2009). Spatially explicit simulation of hydrologically controlled carbon and nitrogen cycles and associated feedback mechanisms in a boreal ecosystem. *Journal of Geophysical Research*, *114*, G02006. http://dx.doi.org/10.1029/2008JG000728.
Gu, L., Falge, E. M., Boden, T., Baldocchi, D. D., Black, T. A., Saleska, S. R., Suni, T., Verma, S. B., Vesala, T., Wofsy, S. C., & Xu, L. (2005). Objective threshold determination for nighttime eddy flux filtering. *Agricultural and Forest Meteorology*, *128*, 179–197.
Hall, F. G., Strebel, D. E., Nickeson, J. E., & Goetz, S. J. (1991). Radiometric Rectification - toward a Common Radiometric Response among Multidate, Multisensor Images. *Remote Sensing of Environment*, *35*, 11–27.
Hall, F. G., Hilker, T., Coops, N. C., Lyapustin, A., Huemmrich, K. F., & Middleton, E. M. (2008). Multi-angle remote sensing of forest light use efficiency by observing PRI variation with canopy shadow fraction. *Remote Sensing of Environment*, *112*, 3201–3211.
Heinsch, F. A., Zhao, M. S., Running, S. W., Kimball, J. S., Nemani, R. R., Davis, K. J., et al. (2006). Evaluation of remote sensing based terrestrial productivity from MODIS using regional tower eddy flux network observations. *Ieee Transactions on Geoscience and Remote Sensing*, *44*, 1908–1925.
Jarvis, P. G., Massheder, J. M., Hale, S. E., Moncrieff, J. B., Rayment, M., & Scott, S. L. (1997). Seasonal variation of carbon dioxide, water vapor, and energy exchanges of a boreal black spruce forest. *Journal of Geophysical Research*, *102*(D24), 28953–28966.
Ju, J. C., & Roy, D. P. (2007). The availability of cloud-free Landsat ETM+ data over the conterminous United States and globally. *Remote Sensing of the Environment*, *112*, 1196–1211.
Jung, M., Reichstein, M., & Bondeau, A. (2009). Towards global empirical upscaling of FLUXNET eddy covariance observations: Validation of a model tree ensemble approach using a biosphere model. *Biogeosciences*, *6*, 2001–2013.
Jung, M., Verstraete, M., Gobron, N., Reichstein, M., Papale, D., Bondeau, A., Robustelli, M., & Pinty, B. (2008). Diagnostic assessment of European gross primary production. *Global Change Biology*, *14*, 2349–2364.
Kalma, J. D., Franks, S. W., & van den Hurk, B. (2001). On the representation of land surface fluxes for atmospheric modeling. *Meteorology and Atmospheric Physics*, *76*, 52–67.
Kim, J., Guo, Q., Baldocchi, D. D., Xu, L., & Leclerc, M. Y. (2006). Upscaling CO_2 fluxes from tower to landscape: Overlaying tower flux footprint calculations on high resolution (IKONOS) vegetation density images. *Agriculture and Forest Meteorology*, *136*, 132–146.
Kljun, N., Kastner-Klein, P., Fedorovich, E., & Rotach, M. W. (2004). Evaluation of Lagrangian footprint model using data from wind tunnel convective boundary layer. *Agricultural and Forest Meteorology*, *127*, 189–201.
Mahrt, L., Vickers, D., & Sun, J. (2001). Spatial variations of surface moisture flux from aircraft data. *Advance Water Resources*, *24*, 1133–1141.
McCaughey, J. H., Pejam, M. R., Arain, M. A., & Cameron, D. A. (2006). Carbon dioxide and energy fluxes from a boreal mixedwood forest ecosystem in Ontario, Canada. *Agricultural and Forest Meteorology*, *140*, 79–96.
Myneni, R. B., Los, S. O., & Asrar, G. (1995). Potential gross primary productivity of terrestrial vegetation from 1982 to 1990. *Geophysical Research Letter*, *22*, 2617–2620.
Papale, D., Reichstein, M., Aubinet, M., Canfora, E., Bernhofer, C., Kutsch, W., Longdoz, B., Rambal, S., Valentini, R., Vesala, T., & Yakir, D. (2006). Towards a standardized processing of net ecosystem exchange measured with eddy covariance technique: algorithms and uncertainty estimation. *Biogeosciences*, *3*, 571–583.
Peichl, M., Brodeur, J. J., Khomik, M., & Arain, M. A. (2010). Biometric and eddy-covariance based estimates of carbon fluxes in an age-sequence of temperate pine forests. *Agricultural and Forest Meteorology*, *150*, 952–965.
Pielke, R. A., Avissar, R., Raupach, M., Dolman, A. J., Zeng, X., & Denning, A. S. (1998). Interactions between the atmosphere and terrestrial ecosystems: Influence on weather and climate. *Global Change Biology*, *4*, 461–475.
Raupach, M. R. (1994). Simplified expressions for vegetation roughness length and zero-plane displacement as functions of canopy height and area index. *Boundary-Layer Meteorology*, *71*, 211–216.
Rebmann, C., Goekede, M., Foken, T., Aubinet, M., Aurela, M., Berbigier, P., Bernhofer, C., Buchmann, N., Carrara, A., Cescatti, A., Ceulemans, R., Clement, R., Elbers, J. A., Granier, A., Grünwald, T., Guyon, D., Havránková, K., Heinesch, B., Knohl, A., Laurila, T., Longdoz, B., Marcolla, B., Markkanen, T., Miglietta, F., Moncrieff, J., Montagnani, L., Moors, E., Nardino, M., Ourcival, J. M., Rambal, S., Rannik, A., Rotenberg, E., Sedlak, P., Unterhuber, G., Vesala, T., & Yakir, D. (2005). Quality analysis applied on eddy covariance measurements at complex forest sites using footprint modelling. *Theoretical and Applied Climatology*, *80*, 121–141.
Reichstein, M., Falge, E., Baldocchi, D., Papale, D., Aubinet, M., Berbigier, P., Bernhofer, C., Buchmann, N., Gilmanov, T., Granier, A., Grünwald, T., Havránková, K., Ilvesniemi, H., Janous, D., Knohl, A., Laurila, T., Lohila, A., Loustau, D., Matteucci, G., Meyers, T., Miglietta, F., Ourcival, J. -M., Pumpanen, J., Rambal, S., Rotenberg, E., Sanz, M., Tenhunen, J., Seufert, G., Vaccari, F., Vesala, T., Yakir, D., & Valentini, R. (2005). On the separation of net ecosystem exchange into assimilation and ecosystem respiration: Review and improved algorithm. *Global Change Biology*, *11*, 1424–1439.
Reichstein, M., Tenhunen, J., Roupsard, O., Ourcival, J. -M., Rambal, S., Miglietta, F., Peressotti, A., Pecchiari, M., Tirone, G., & Valentini, R. (2003). Inverse modeling of seasonal drought effects on canopy CO_2/H_2O exchange in three Mediterranean ecosystems. *Journal of Geophysical Research*, *108*, 4726–4742.
Richardson, A. D., Hollinger, D. Y., Burba, G. G., Davis, K. J., Flanagan, L. B., Katul, G. G., Munger, J. W., Ricciuto, D. M., Stoy, P. C., Suyker, A. E., Verma, S. B., & Wofsy, S. C. (2006). A multi-site analysis of random error in tower-based measurements of carbon and energy fluxes. *Agricultural and Forest Meteorology*, *136*, 1–18.
Running, S. W., Baldocchi, D. D., Turner, D., Gower, S. T., Bakwin, P., & Hibbard, K. (1999). A global terrestrial monitoring network, scaling tower fluxes with ecosystem modeling and EOS satellite data. *Remote Sens. Environ.*, *70*, 108–127.
Schmid, H. P. (1994). Source areas for scalar and scalar fluxes. *Boundary-Layer Meteorology*, *67*, 293–318.
Schmid, H. P., & Lloyd, C. R. (1999). Spatial representativeness and the location bias of flux footprint over inhomogeneous areas. *Agriculture and Forest Meteorology*, *93*, 195–209.
Sellers, P. J. (1985). Canopy reflectance, photosynthesis and transpiration. *International Journal of Remote Sensing*, *6*, 1335–1372.
Şen, Z. (1998). Point Cumulative Semivariogram for Identification of Heterogeneities in Regional Seismicity of Turkey. *Mathematical Geology*, *30*, 767–787.
Sertel, E., Kaya, S., & Curran, P. J. (2007). Use of semivariograms to identify earthquake damage in an urban area. *Ieee Transactions on Geoscience and Remote Sensing*, *45*, 1590–1594.
Slaymaker, D. M., Jones, K. M. L., Griffin, C. R., & Finn, J. T. (1996). Mapping deciduous forests in southern New England using aerial videography and hyperclustered multi-temporal Landsat TM imagery, Gap Analysis: A Landscape Approach to Biodiversity Planning. In J. M. Scott, T. Tear, & F. Davis (Eds.), *Proceedings of the ASPRSIGAP Symposium, National Biological Service, Moscow, Idaho* (pp. 87–101).
Soegaard, H., Jensen, N. O., Boegh, E., Hasager, C. B., Schelde, K., & Thomsen, A. (2003). Carbon dioxide exchange over agricultural landscape using eddy correlation and footprint modelling. *Agricultural and Forest Meteorology*, *114*, 153–173.
Sogachev, A., Rannik, U., & Vesala, T. (2004). Flux footprints over complex terrain covered by heterogeneous forest. *Agricultural and Forest Meteorology*, *127*, 143–158.
Song, C. H., & Woodcock, C. E. (2002). The spatial manifestation of forest succession in optical imagery - The potential of multiresolution imagery. *Remote Sensing of Environment*, *82*, 271–284.
Stull, R. B. (1988). *An introduction to boundary layer meteorology*. Norwell, MA: Kluwer Acad 666 pp.
Syed, K. H., Flanagan, L. B., Carlson, P. J., Glenn, A. J., & Van Gaalen, K. E. (2006). Environmental control of net ecosystem CO_2 exchange in a treed, moderately rich fen in northern Alberta. *Agricultural and Forest Meteorology*, *140*, 97–114.
Tucker, C. J. (1979). Red and photographic infrared linear combinations for monitoring vegetation. *Remote Sensing of Environment*, *8*, 127–150.
Turner, D. P., Urbanski, S., Bremer, D., Wofsy, S. C., Meyers, T., Gower, S. T., & Gregory, M. (2003). A cross-biome comparison of daily light use efficiency for gross primary production. *Global Change Biology*, *9*, 383–395.
Weaver, L. A., Flanagan, L. B., & Carlson, P. J. (2002). Seasonal and interannual variation in evapotranspiration, energy balance, and surface conductance in a northern temperate grassland. *Agricultural and Forest Meteorology*, *112*, 31–49.
Wilson, K. B., & Baldocchi, D. D. (2000). Seasonal and interannual variability in energy fluxes over a broadleaved temperate deciduous forest in North America. *Agricultural and Forest Meteorology*, *100*, 1–18.
Woodcock, C. E., Strahler, A. H., & Jupp, D. L. B. (1988). The Use of Variograms in Remote-Sensing 1. *Scene Models and Simulated Images. Remote Sensing of Environment*, *25*, 323–348.
Wu, J. D., Wang, D., & Bauer, M. E. (2005). Image-based atmospheric correction of QuickBird imagery of Minnesota cropland. *Remote Sensing of Environment*, *99*, 315–325.
Wulder, M. A., Dechka, J. A., Gillis, M. A., Luther, J. E., Hall, R. J., & Beaudoin, A. (2003). Operational mapping of the land cover of the forested area of Canada with Landsat data: EOSD land cover program. *Forestry Chronicle*, *79*, 1075–1083.
Wulder, M. A., White, J. C., Magnussen, S., & McDonald, S. (2007). Validation of a large area land cover product using purpose-acquired airborne video. *Remote Sensing of Environment*, *106*, 480–491.
Wulder, M. A., White, J. C., Goward, S. N., Masek, J. G., Irons, J. R., Herold, M., et al. (2008). Landsat continuity: Issues and opportunities for land cover monitoring. *Remote Sensing of Environment*, *112*, 955–969.
Xing, Z., Bourque, C. P. -A., Meng, F., Zha, T., Cox, R. M., & Swift, D. E. (2007). A simple net ecosystem productivity model for gap filling of tower-based fluxes: An extension of Landsberg's equation with modifications to the light interception term. *Ecological Modelling*, *206*, 250–262.
Yang, L., Ichii, K., White, M. A., Hashimoto, H., Michaelis, A., Votava, P., Zhu, A., et al. (2007). Developing a continental-scale measure of gross primary production by combining MODIS and AmeriFlux data through Support Vector Machine approach. *Remote Sensing of Environment*, *110*, 109–122.
Yates, D. N., Chen, F., & Nagai, H. (2003). Land surface heterogeneity in the Cooperative Atmosphere-Surface Exchange Study (CASES-97). Part II: Analysis of spatial heterogeneity and its scaling. *Journal of Hydrometeorology*, *4*, 219–234.